Spectrochimica Acta Part A: Molecular and Biomolecular Spectroscopy 227 (2020) 117664

Contents lists available at ScienceDirect

Spectrochimica Acta Part A: Molecular and Biomolecular Spectroscopy

journal homepage: www.elsevier.com/locate/saa

Plasmonic cellulose textile fiber from waste paper for BPA sensing by SERS

Sijia Liu [a], Rongkai Cui [a], Yibo Ma [b], Qian Yu [a, **], Akash Kannegulla [c], Bo Wu [c], Hongtao Fan [a], Alan X. Wang [c], Xianming Kong [a, *]

[a] College of Chemistry, Chemical Engineering and Environment Engineering, Liaoning Shihua University, Fushun, Liaoning, 113001, PR China
[b] Department of Bioproducts and Biosystems, School of Chemical Engineering, Aalto University, 00076, Aalto, Finland
[c] School of Electrical Engineering and Computer Science, Oregon State University, Corvallis, OR, 97331, USA

ARTICLE INFO

Article history:
Received 9 May 2019
Received in revised form
13 October 2019
Accepted 14 October 2019
Available online 19 October 2019

Keywords:
Cellulose textile fiber
Flexible sensor
Plasmonic NPs
BPA
SERS

ABSTRACT

Flexible plasmonic Surface-enhanced Raman scattering (SERS) substrates were fabricated using cellulose textile fibers, in which the textile fibers were recycled from waste paper in an eco-friendly way. The Glycidyltrimethylammonium chloride (GTAC) with positive charges was grafted onto the surface of the cellulose textile fibers through cationization. Plasmonic silver nanoparticles (Ag NPs) with negative charges were decorated onto the cellulose textile fibers via electrostatic interactions. After cationization, the variation range of the diameter of the cellulose textile fibers was significantly increased because part of the cellulose was dissolved under alkaline condition, leading to more 'hot spots' for SERS during the shrinking process. The cellulose textile fiber-Ag NPs nanocomposite was employed for monitoring bisphenol A (BPA) in water and soft drink by SERS and the sensitivity of BPA detection achieved 50 ppb. The recovery values of BPA in soda water samples were from 96% to 105%. These results illustrate that the cellulose textile fiber-Ag NPs nanocomposite can be used as flexible, high sensitivity SERS substrates for detecting harmful ingredients in food or environment.

1. Introduction

Surface-enhanced Raman scattering (SERS) spectroscopy is a powerful analytical technique and has attracted considerable interests in recent decades [1]. SERS could gather molecule vibrational information of analyte at trace concentration even down to the single-molecule level [2–4], which enables SERS to play significant roles in many analytical applications, such as biosensing, food safety, environment monitoring and forensic sciences [5–9]. The outstanding sensitivity of SERS is mainly associated with the electromagnetic field from localized surface plasmon resonance (LSPR) and the charge transfer between the targets and metallic substrate [10–12]. During the last two decades, developing efficient SERS substrates was one of the most important topics in SERS techniques [13]. Numerous strategies have been proposed to prepare plasmonic substrates with good SERS enhancement, such as silver nanocubes, silver nanowire film, bimetallic nanoparticles and 2D materials with Ag nanoarrays [14–17]. Most of these prepared SERS substrates are rigid, which are usually fragile and inconvenient for detecting analytes on the surface of irregularly shaped objects. Therefore, it is necessary to develop a flexible substrate with plasmonic nanomaterials for SERS sensing. Compared with conventional rigid SERS substrates, flexible substrates will emerge as a new generation of sensing platforms which can be directly applied in monitoring analytes from irregularly shaped surface and more 'hot spots' for SERS could be formed due to the flexible feature.

Several kinds of flexible substrates including polymer films, graphene oxide sheets, filter paper and cotton fabrics were employed for flexible SERS substrates [18–21]. Cellulose-based SERS substrates have attained considerable interests of researchers, as their cost-effective, environmental friendly and renewable [22]. Park. et al. decorated cellulose paper with bimetallic Au/Ag nanocomposites and used it as active flexible SERS substrate, which could provide picomolar detection limit of folic acid [20]. Lin's group have taken advantage of cellulose nanofiber as flexible support and deposited Au NPs through electrostatic interaction used as SERS substrates, which exhibited good performance in food safety sensing [23,24]. The recycled cellulose fabric fiber from waste paper or cardboard is a viable material in modern world

---

* Corresponding author.
** Corresponding author.
E-mail addresses: qyu@lnpu.edu.cn (Q. Yu), xmkong@lnpu.edu (X. Kong).

https://doi.org/10.1016/j.saa.2019.117664

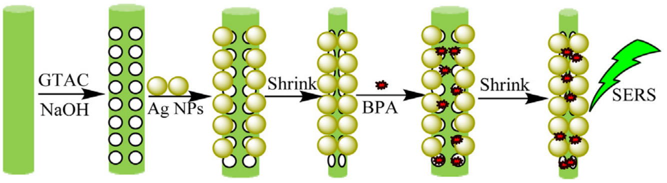

Scheme 1. Illustration of fabrication of flexible plasmonic cellulose textile fiber for BPA sensing.

because it not only supports the man-made cellulosic fabrics but also provides a new way for landfill recycling. Ma et al. used advanced strategy named Ioncell-F method, which prepare cellulose fabrics from waste paper and cardboard by using ionic liquid as solvent [25].

Endocrine-disrupting compounds (EDCs) are chemicals from organic synthesis or nature, which are harmful for the health of humans and animals through affecting the endocrine system. EDCs are esteemed to be a critical factor of reproductivity and sexual disorders in wildlife [26]. Several types EDCs are released into the aquatic system of the environment. Even at low concentrations, EDCs also could bring serious problems to the endocrinium of humans and wildlife. BPA is subcategory molecule of EDCs which can show estrogenic toxicity in contaminated water [27,28]. Various analytical technologies have been developed for the identification of BPA, including gas-liquid chromatography, fluorescence spectroscopy, high performance liquid chromatography and electrochemical biosensor [29–32]. However, these technologies are time-consuming, require skilled personnel and the extraction or pretreatment processes of sample are indispensable. SERS methods have been employed for BPA sensing. Feng et al. fabricated gold nanoparticle-nanorod heteroassemblies and used for BPA sensing, the limit of detection was down to 3.9 pg/mL [33]. Yang et al. has successfully detected BPA from milk product by using halides modified Au nanoparticles as the SERS substrates [34]. These SERS methods are reliable and sensitive for monitoring BPA, but the surface modification is indispensable.

In this study, we fabricated flexible, low-cost, simple and efficient fabric SERS substrates, in which the flexible cellulose textile fibers were recycled from waste paper and used as the solid support. The Ag NPs are decorated on the surface of the fibers via electrostatic interaction. The flexible feature of cellulose textile fiber could change the distance between Ag NPs dramatically and more clusters of Ag NPs could be formed during the shrinking process. This cellulose textile fiber-Ag NPs composite was employed for identification of BPA in aerated drinks. Several merits of such SERS substrates make it suitable for in-situ monitoring and identification of harmful ingredients in the environment. First, the cellulose textile fiber recycled from waste paper is eco-friendly and cost effective. Second, more ‘hot spots’ for SERS could be formed during the shrinking process. Third, the surface modification of fiber-Ag NPs is unnecessary as the pore of fiber could adsorb BPA during the swelling process. The proof-of-concept measurement exhibited that the textile fiber-Ag NPs composite could be applied for monitoring water contamination.

2. Experimental

2.1. Materials and chemicals

Bisphenol A (BPA) and sodium hydroxide (NaOH) were obtained from Sinopharm Chemical Reagent Co., Ltd (China). Glycidyltrimethylammonium chloride (GTAC), 4-mercaptobenzoicacid (MBA), poly-diallyldimethylammonium chloride (PDDA), thiram, silver nitrate ($AgNO_3$) and trisodium citrate ($Na_3C_6H_5O_7$) was purchased from Aladdin (Shanghai, China), p-Aminothiophenol (PATP) was obtained from Innochem (Beijing, China). All the chemicals were used as received in the experiment without any purification. The cellulose textile fiber recycling from waste paper through IONCELL-F technology was supplied by Sixta’s Group at Aalto University, the detail of IONCELL-F technology was described in their

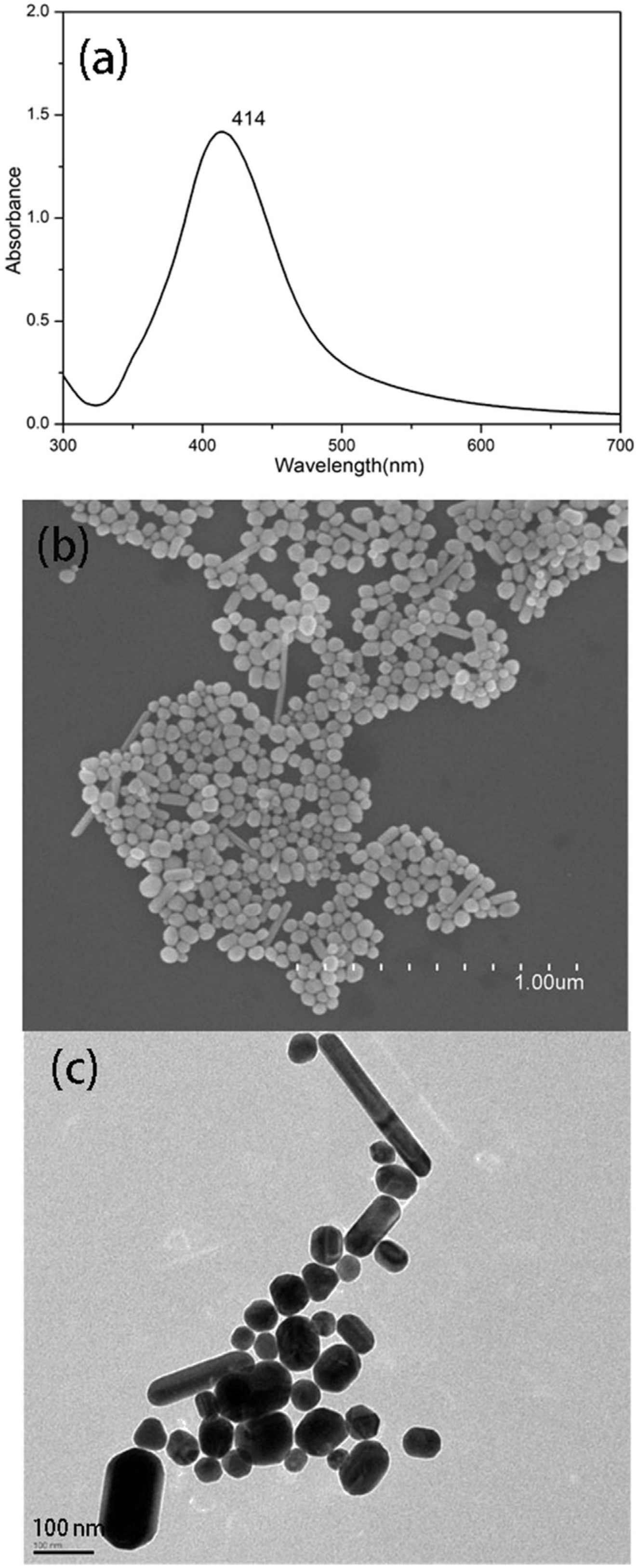

Fig. 1. UV–vis spectrum(a), SEM(b) and TEM(c) images of Ag NPs.

previous publications [25,35,36], in which the ionic liquid 1,5-diazabicyclo[4.3.0]non-5-ene acetate ([DBNH][OAc]) was used for dissolving cellulose. The water used through study was double distilled (resistivity ~ 18.2 MΩ cm). The process of the experiment was schematically presented in Scheme 1.

2.2. Silver nanoparticles preparation

The Ag colloid were prepared according the typical method proposed by Lee et al. with a minor modification [37]. The trisodium citrate was used as capping and reducing agent. Briefly, the solid $AgNO_3$ (0.035 g) were dissolved in 200 mL of ultrapure water and the solution was heated to reflux under vigorous stirring. Then

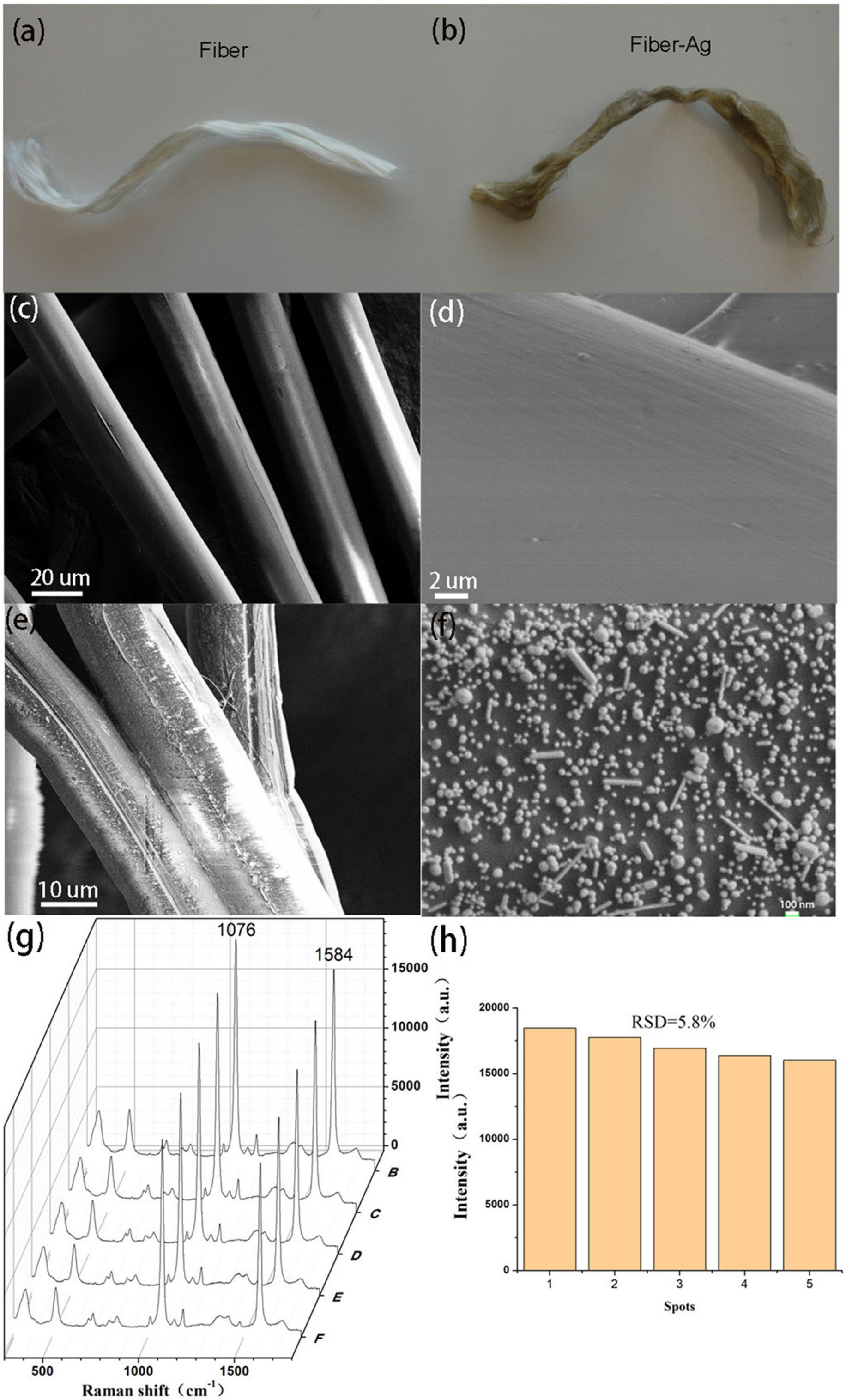

Fig. 2. Photographic images of cellulose textile fiber (a),(b) and SEM images of cellulose textile fiber (c), (d) and after Ag NPs decoration (e), (f), the SERS spectra of MBA (10 ppm) collected from five random spots of the fiber-Ag substrate (c) and the histogram results of the intensities at the 1584 cm^{-1} peak (d).

sodium citrate aqueous solution (3.8 mL of 1%) was added to the system. The mixture solution was kept reflux for 1 h. After cool down to room temperature the colloidal Ag NP suspension with green appearance was obtained and kept in refrigerator for further using. The glassware used in the study was firstly soaked with aqua regia solution (HNO_3/HCl, 1:3, v/v) and followed by washed thoroughly with ultrapure water.

2.3. *Surface modification of cellulose textile fibers*

The cellulose textile fiber was surface-modified with positive charges for decorating Ag NPs. The process was according to the method reported by Castellanos et al. with a minor modification [38]. Glycidyltrimethylammonium chloride (GTAC) has positive charges due to their quaternary ammonium groups and was grafted onto cellulose textile fibers under alkaline conditions. NaOH (1.5 g) was dissolved in 15 mL of ultra-pure water and 3 mL of GTAC were added into the mixture. Cellulose textile fibers (0.1 g) were added into the mixture solution and immersing for 20 min, then the textile fibers were taking out by tweezers and rinsing with ultra-pure water triply.

2.4. *Self-assembly of plasmonic Ag NPs on cellulose textile fiber*

The plasmonic Ag NPs were decorated onto the surface of cellulose textile fibers through electrostatic self-assembly process. The GTAC modified cellulose textile fiber (10 mg) were immersed in pure water for 5 min, and then transferred into Ag colloids (10 mL) with original concentration. After 10 min the fibers were taking out by tweezers and washing thoroughly with ultra-pure water.

2.5. *SERS sensing of the specimens*

SERS performance of the cellulose textile fibers coated with Ag NPs (fiber-Ag) were investigated using aqueous solution of PATP, a typical Raman probe molecule. The fiber-Ag substrate was dipped in 1 mL of PATP aqueous solutions with different concentrations for 3 min and then dried in air. Same procedure was used for BPA SERS sensing. In order to achieve convenient on-site detection, the Raman measurements were carried out using portable Raman spectrometer (BWS465 iRman; B&W Tek, USA) with an excitation laser of 785 nm and with 5 cm^{-1} resolution. The diameter of the beam spot was 105 μm and a 1.5 m bifurcated fiber probe was used to illuminate the sample and collect the Raman signals. Raman spectra were recorded by the BWSPEC Software. The SERS spectra were processed and plotted using Origin software (version 8.0). Five spectra were collected from different spots of each fiber-Ag substrate (N = 5).

2.6. *Other measurements*

Scanning electron microscopy (SEM) images were acquired on SU8010 field emission scanning electron microscope (Hitachi, Japan), transmission electron microscopy (TEM) analysis of Ag NPs was developed using a JEM-2100F electron microscope (JEOL, Japan). UV—vis absorption spectra of Ag colloid were acquired on a Lambda 900 UV—Vis—NIR spectrophotometer (PerkinElmer, USA) using quartz cells of 10 mm optical path. X-ray diffraction analysis of fiber samples were conducting on X-ray powder diffractometer (PANalytical X'Pert PRO, Cu $K_{\alpha 1}$, 0.0262606° resolution, Malvern Panalytical, UK). The fibers and fiber-Ag samples were made to suitable size pellets for the measurements.

3. Results and discussion

3.1. *Sample fabrication and characterization*

The sodium citrate is one of typical reducing agents for preparing Ag colloid used for SERS application. The sodium citrate was also used as stabilizer of the colloidal Ag NPs [39] and the negative charges on the surface of Ag NPs could bound to the surface with positive charges through electrostatic interaction. In this research, the Ag NPs were synthesized by citrate reduction method. The prepared Ag NPs exhibited obvious plasmonic features in the UV—Vis spectra at 414 nm as shown in Fig. 1(a). The morphological information of the Ag NPs was determined by SEM and TEM images

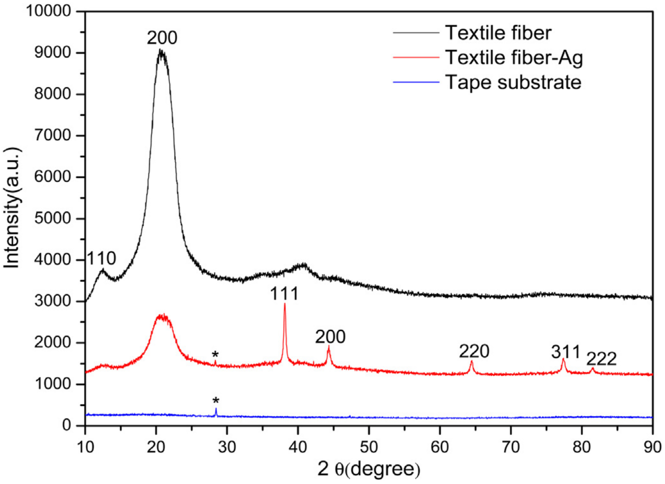

Fig. 3. XRD patterns of cellulose textile fiber, fiber-Ag composite materials and the tape used for hold sample.

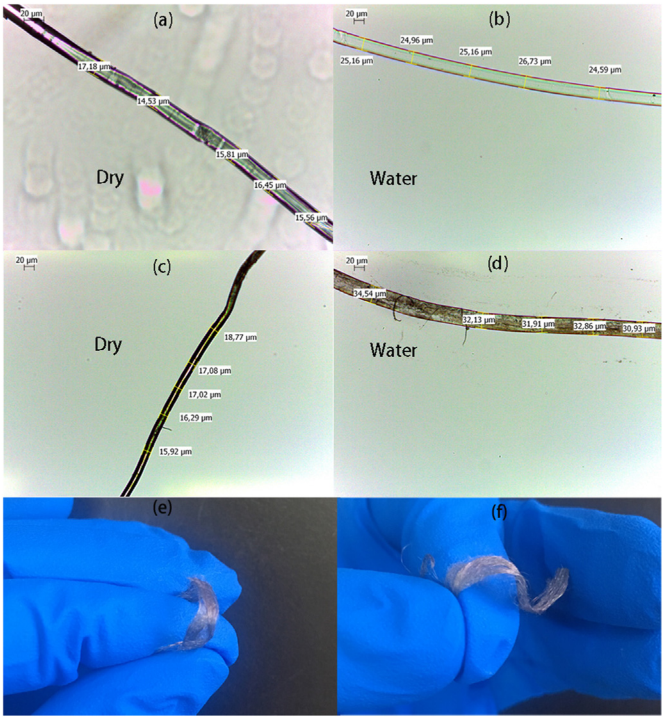

Fig. 4. Microscopic images of cellulose textile fibers (a), (b), and after grafting GTAC with Ag NPs assembled fiber-Ag composite (c), (d) under dried or water conditions, (e) and (f) depict the flexibility of cellulose textile fibers-Ag composite.

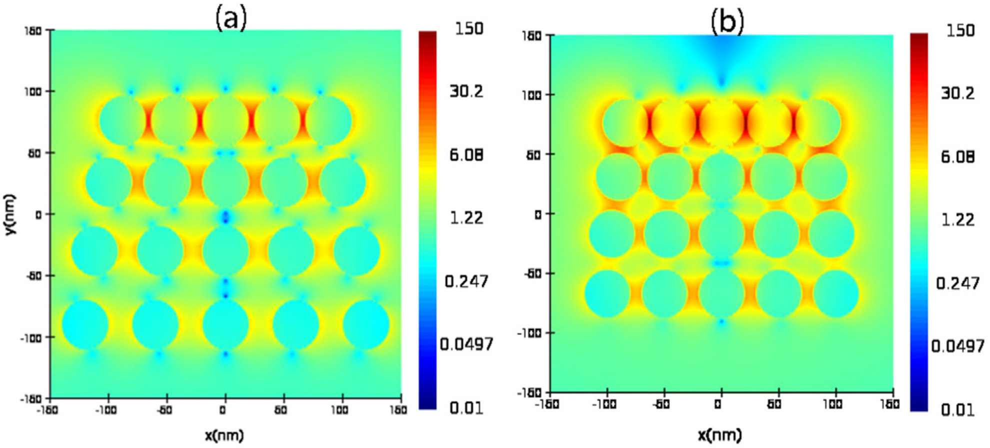

Fig. 5. FDTD simulation of electric field intensity (logarithmic $|E/E_0|^2$) at certain area under the excitation laser's wavelength (785 nm) for Ag NPs on fiber under swelling (a) and shrink condition(b).

(Fig. 1 b and c). The prepared Ag NPs have spherical or round morphology and the diameters were between 40-60 nm, several nanorods were observed. In order to evaluate the uniformity of Ag NPs, SERS spectra at five randomly spots of glass-Ag are presented in Fig. S1a. The five SERS spectra of MBA display nearly at similar intensities Fig. S1b, which mean the Ag NPs using for SERS sensing is acceptable.

The appearance of the colloidal Ag used in the experiment was yellowish-green (Fig. S2). The appearance of the cellulose textile fiber and after Ag NPs decorating was shown in Fig. 2(a) and (b). The color of original cellulose textile fiber was white which is similar to cotton fabrics. After decorating Ag NPs onto the surface of cellulose textile fibers, the color of textile fiber becomes grey due to the surface plasmon resonance effects of Ag NPs. SEM images elaborates the features of textile fiber's surface. Fig. 2 (c) illustrates several cellulose textile fibers, which shows a fibrillary structure with diameter of 18 μm. Fig. 2(d) provides the specific topographical surface of the cellulose textile fibers, that is very clean before the bonding of Ag NPs. When the Ag NPs were assembled onto the surface of cellulose textile fibers via electrostatic interaction as shown in Fig. 2(e), the surface of cellulose textile fibers becomes roughened but the fiber diameters remains unchanged. The Ag presence on the surface of fiber-Ag sample was also investigated by the energy dispersive X-ray (EDX) analysis under SEM as provided in Fig. S3, in which distinctive peaks of Ag were observed. Fig. 2 (f) shows that the Ag NPs are randomly deposited on the whole surface of the cellulose textile fiber. The clusters of Ag NPs on the fiber surface are significantly beneficial to SERS enhancement. The image and diameter distribution of the fibers (20 fibers) were shown in Fig. S4 (20 fibers were measured as only 22 fibers within the field of view). The average value of the diameter is 15.2 μm with the standard deviation at 1.3 μm. The uniformity of SERS signals across the fiber-Ag substrate are shown in Fig. 2 and the relative standard deviation (RSD) of five spots from the fiber-Ag is 5.8%, which indicated the fiber-Ag composite are suitable for use in SERS sensing. The variation of SERS enhancement from fiber with different diameters is negligible.

In order to further verify the decoration of Ag NPs on the textile fiber's surface and their phase and crystallinity, XRD spectra were collected. The XRD spectra collected from cellulose textile fiber, fiber-Ag composites and the blank tape (used as substrate for holding sample) are shown in Fig. 3. In the case of blank cellulose textile fiber, a small bump at 2θ values of 12.5 and an intense peak at $2\theta = 20.5$ were observed. These two peaks are assigned to the (110) and (200) planes of cellulose II. After the AgNPs decorating onto the surface of textile fiber, the fiber-Ag composite exhibited one broad band at $2\theta = 20.5$ and five new obvious peaks at 2θ values of 38.3°, 44.5°, 64.7°, 77.6°, and 81.7° were observed, the five new peaks are assigned to Ag crystals because they correspond to the diffraction planes of (111), (200), (220) (311) and (311) of metal silver, (JCPDS card Ag: No. 04–0783). The tiny peaks labeled with asterisk marks are results from the tape substrate, which have no interference to the measurement. This further proved that the metallic crystalline Ag NPs that are decorated on the surface of textile fiber successfully, which are in agreement with the bird-eye and SEM images.

It is noteworthy that the textile fiber not only has outstanding mechanical flexibility but also exhibits the excellent stretching feature of diameter. The Microscopic images in Fig. 4 shown the stretching feature of textile fiber under dry and water condition. The average diameter of cellulose textile fiber is around 16 μm under dry condition as shown in Fig. 4 (a). When dropping water onto the cellulose textile fiber, the diameter increased to nearly 25 μm (Fig. 4 b). This increment was attributed to the water molecule penetrated into the amorphous area of cellulose textile fiber. After cationized with GTAC under strong alkaline condition, the Ag NPs were decorated onto the surface of cationized cellulose textile fiber and the diameter of fiber-Ag almost no difference compared with cellulose textile fiber as shown in Fig. 4(c). When the textile fiber-Ag encountered with water, the diameter increased to nearly 32 μm. The significant increase in the diameter of the textile fiber-Ag was induced by much more amount of water penetrating into the free space of textile fiber-Ag composite. Because the cellulose matrix in textile fibers were partly dissolved under the strongly alkaline condition for fiber cationizing and more free space was created on the textile fiber. During the shrinking process of textile fiber-Ag, the distance between Ag NPs was decreased and more "hotspots" for SERS would be formed [40]. Furthermore, the target molecules were adsorbed onto the surface of fiber during the shrinking process, which could enrich analytes near the plasmonic Ag NPs. The fiber-Ag shown better SERS performance at shrink condition than that at swelling condition (Fig. S5). The textile fiber-Ag composites possessed excellent flexibility as shown in Fig. 4(e) and (f), these nanocomposites could be folded into any shapes randomly, that feature enable fiber-Ag SERS substrate has potential to detect analyte from the curved surface.

3.2. Electromagnetic field simulation

Finite-difference time-domain (FDTD) theoretical simulations were developed to evaluate the local electromagnetic fields at certain area (140 nm × 140 nm) under the excitation laser's

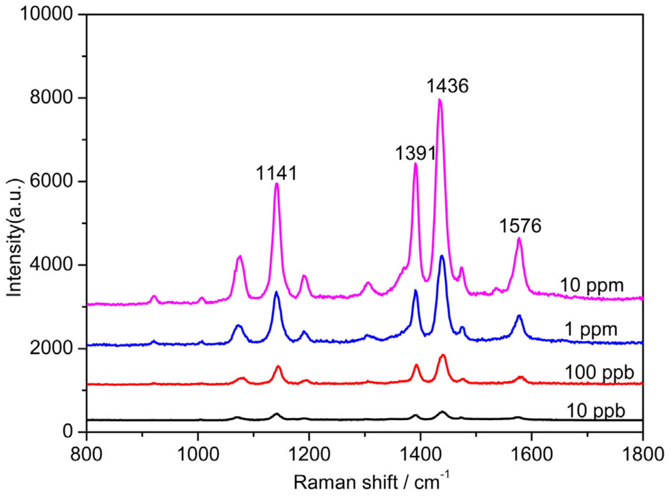

Fig. 6. SERS spectra of cellulose textile fiber-Ag composite dipped out from different concentrations of PATP solutions.

wavelength (785 nm) for Ag NPs with different distance, the polarization of light is along x-axis. In order to run the simulation closer to the real situation, the gap distances of Ag NPs on the fiber were set as 4 nm, 10 nm, 16 nm and 20 nm in swelling condition (Fig. 5(a)) and 2 nm, 5 nm, 8 nm and 10 nm in dry condition (Fig. 5(b)). The electric field distribution ($|E/E_0|$) (here E is local electric field of the Ag nanostructure and E_0 is the amplitude of the incident light) of Ag nanostructures were shown in Fig. 5. The average intensity value of the electric field (logarithmic $|E/E_0|^2$) at the certain area is 12 and 22.3 corresponding to swelling and dry condition of fiber-Ag respectively. The significant increment of electric field was result from the highly concentrated electromagnetic fields associated with LSPR at interstitial sites (hot spots) in cluster consisting of two coupled Ag nanoparticles (shrink under dry condition). The simulations results prove that more ‘hot spots’ for SERS could formed during the shrinking process of the cellulose textile fibers-Ag substrate.

3.3. SERS measurement

In order to evaluate the SERS performance of cellulose textile fibers-Ag composite, a common Raman reporter molecule PATP was employed as analyte. The textile fibers-Ag composite was immersed in aqueous solution of PATP at various concentration and the Raman signals were collected as shown in Fig. 6. The SERS peaks of 4,4′-dimercaptoazobenzene (DMAB) were observed. When the laser illuminated onto the surface of silver with PATP assembled during the process of SERS measurement, the photocatalytic coupling reactions happened and yield a new species of DMAB [41,42]. DMAB possess higher Raman cross section than that from PATP and gives four intense Raman peaks at 1141, 1391, 1436 and 1576 cm^{-1}. The peak at 1141 cm^{-1} is assigned to the β(CH) mode. The 1391 and 1436 cm^{-1} peaks are assigned to the N=N stretching mode and 1576 cm^{-1} is assigned to benzene ring of DMAB [11,43]. As shown in Fig. 6, the feature peaks of the DMAB present a monotonous decrease in intensity as the concentration decrease. Distinct Raman peaks are still observed even down to the 10-ppb level. The gold nanoparticles also could be assembled on the surface of textile fiber and show SERS activity. As the cost of gold is higher than silver and the Ag NPs show higher SERS efficiency than Au NPs, we chose Ag NPs in this study for further applications.

As a kind of chemical compound, BPA is usually used as additive to manufacture plastics and resins. The BPA is positively related to cardiovascular disease and bring the problem of reproductive capacity of adults. The Commission Regulation of EU has strengthening the migration limit for BPA from 0.6 ppm to 0.05 ppm in food contact plastics [44]. Herein, the cellulose textile fiber-Ag

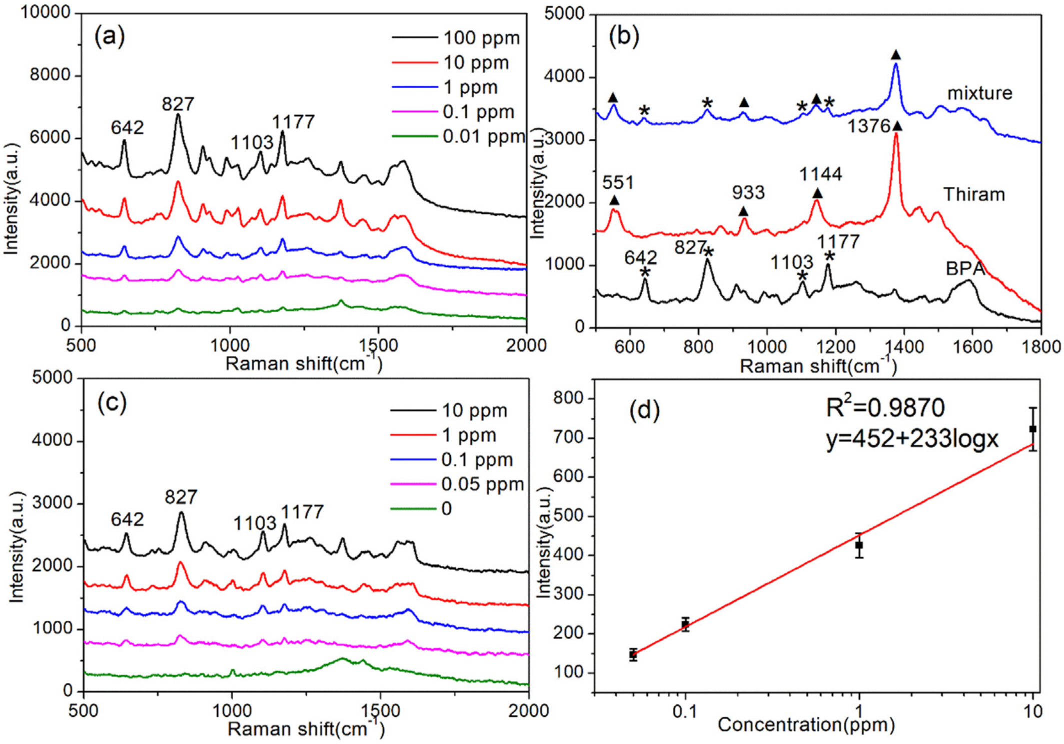

Fig. 7. SERS spectra of cellulose textile fiber-Ag composite dipped out from aqueous solution (a) and Soda water (c) with different concentrations of BPA and the intensities of Raman peaks at 827 cm^{-1} as a function of logarithm of BPA concentrations from Soda water (d), (b) SERS spectra of 1 ppm of thiram and BPA and their mixture sample (1 ppm of BPA and 1 ppm of thiram, equal volume, the triangle-labeled peaks are assigned to thiram and the asterisk-labeled peaks are assigned to BPA).

composite was employed for BPA SERS sensing. Fig. 7(a) shows the Raman spectra collected by dipped cellulose textile fiber-Ag composite into various concentrations of BPA aqueous solution. The Raman peaks around 642, 827, 1103 and 1177 cm^{-1} were observed clearly, that are in accordance with the reported work [45]. The Raman intensity decreased with the decreasing concentrations of BPA (100 ppm to 0.01 ppm). To evaluate the advantage of the textile fiber-Ag substrate, another rigid SERS substrate was fabricated by assembling Ag NPs on glass slides and used for BPA sensing. Fig. S6 shows that at a concentration of 0.1 ppm nearly no SERS signal of BPA was observed using the glass substrate. The predominant SERS performance of flexible fiber-Ag was due to more 'hot spot' and more BPA molecule captured during the shrink process of textile fiber. In order to investigate the interference from other molecules, we added other EDCs(thiram) into the BPA solution and measured the SERS spectra of the mixed sample. Since the Raman peaks of Thiram(triangle-labeled) and BPA (asterisk-labeled) have no overlap, both of these two compounds can be detected with featured Raman spectra shown in Fig. 7(b). This SERS substrate was also used for sensing BPA from Soda water as shown in Fig. 7(c). When the concentration down to limitation of EU (0.05 ppm), obvious Raman signals of BPA are still observed. The sensitivity is comparable with other systems [34] and the surface functionalization was not necessary here as the BPA could be captured by the swelling process of cellulose fiber. Fig. 7(d) presents the quantitative relation between the concentration of BPA and the intensity of feature Raman peak at 827 cm^{-1}, which present a good linear relationship between the peak intensity and the concentration of the BPA from soda water. The recovery values of BPA in soda water samples were from 96% to 105% (see Electronic Supplementary Material Table S1), these results validate that this proposed method can be used for monitoring BPA from soda water. This study would facilitate the development of flexible SERS substrates base on cellulose fabrics.

4. Conclusion

In summary, flexible and high sensitivity SERS substrates were fabricated through assembling Ag nanoparticles onto cellulose textile fibers. The textile fibers were eco-friendly as they were recycled from waste paper by IONCELL-F technology. The cellulose textile fibers play a critical role in such SERS substrates because they not only provide solid support for high density Ag NPs, but also offer shrinking and swelling process to reduce the gaps between Ag NPs. The LSPR couplings at the junction of Ag NPs make it possible for the significant enhancement of the electric field for SERS, which offer more hot spots. Proof of concept SERS application of such flexible plasmonic substrates was verified by detecting BPA in DI water and aerated water. This cellulose textile fiber-Ag nanocomposite is promising for quantitative detection of BPA from drinks.

Declaration of competing interest

The authors declare that they have no conflict of interest.

Acknowledgement

The authors would like to acknowledge the support from the Natural Science Foundation of Liaoning Province China (No. 20180550246), the talent scientific research fund of LSHU, China (No. 2017XJJ-037), and Liaoning Shihua University Student's project for Innovation and Entrepreneurship Training Program, China (201810148065), the United States National Institutes of Health under Grant No. 1R21DA0437131 and the Unites States Department of Agriculture under Grant No. 2017-67021-26606.

Appendix A. Supplementary data

Supplementary data to this article can be found online at https://doi.org/10.1016/j.saa.2019.117664.

References

[1] B. Liu, D. Zhang, H. Ni, D. Wang, L. Jiang, D. Fu, X. Han, C. Zhang, H. Chen, Z. Gu, Multiplex analysis on a single porous hydrogel bead with encoded SERS nanotags, ACS Appl. Mater. Interfaces 10 (2017) 21–26.
[2] S. Nie, S.R. Emory, Probing single molecules and single nanoparticles by surface-enhanced Raman scattering, Science 275 (1997) 1102–1106.
[3] H. Xu, E.J. Bjerneld, M. Käll, L. Börjesson, Spectroscopy of single hemoglobin molecules by surface enhanced Raman scattering, Phys. Rev. Lett. 83 (1999) 4357.
[4] K. Kneipp, Y. Wang, H. Kneipp, L.T. Perelman, I. Itzkan, R.R. Dasari, M.S. Feld, Single molecule detection using surface-enhanced Raman scattering (SERS), Phys. Rev. Lett. 78 (1997) 1667.
[5] C. Fu, Y. Wang, G. Chen, L. Yang, S. Xu, W. Xu, Aptamer-based surface-enhanced Raman scattering-microfluidic sensor for sensitive and selective polychlorinated biphenyls detection, Anal. Chem. 87 (2015) 9555–9558.
[6] X. Kong, Q. Yu, E. Li, R. Wang, Q. Liu, A.X. Wang, Diatomite photonic crystals for facile on-chip chromatography and sensing of harmful ingredients from food, Materials 11 (2018) 539.
[7] C. Muehlethaler, M. Leona, J.R. Lombardi, Review of surface enhanced Raman scattering applications in forensic science, Anal. Chem. 88 (2015) 152–169.
[8] P. Wang, S. Pang, B. Pearson, Y. Chujo, L. McLandsborough, M. Fan, L. He, Rapid concentration detection and differentiation of bacteria in skimmed milk using surface enhanced Raman scattering mapping on 4-mercaptophenylboronic acid functionalized silver dendrites, Anal. Bioanal. Chem. 409 (2017) 2229–2238.
[9] C. Wang, Z. Zhang, L. He, Development of a headspace solid-phase microextraction–surface-enhanced Raman scattering approach to detect volatile pesticides, J. Raman Spectrosc. 50 (2018) 6–14.
[10] K.A. Willets, R.P. Van Duyne, Localized surface plasmon resonance spectroscopy and sensing, Annu. Rev. Phys. Chem. 58 (2007) 267–297.
[11] X. Kong, Q. Yu, Z. Lv, X. Du, Tandem assays of protein and glucose with functionalized core/shell particles based on magnetic separation and surface-enhanced Raman scattering, Small 9 (2013) 3259–3264.
[12] J. Wang, W. Lin, X. Xu, F. Ma, M. Sun, Plasmon-exciton coupling interaction for surface catalytic reactions, Chem. Rec. 18 (2018) 481–490.
[13] A.X. Wang, X. Kong, Review of recent progress of plasmonic materials and nano-structures for surface-enhanced Raman scattering, Materials 8 (2015) 3024–3052.
[14] J.M. McLellan, Z.-Y. Li, A.R. Siekkinen, Y. Xia, The SERS activity of a supported Ag nanocube strongly depends on its orientation relative to laser polarization, Nano Lett. 7 (2007) 1013–1017.
[15] A. Tao, F. Kim, C. Hess, J. Goldberger, R. He, Y. Sun, Y. Xia, P. Yang, Langmuir–Blodgett silver nanowire monolayers for molecular sensing using surface-enhanced Raman spectroscopy, Nano Lett. 3 (2003) 1229–1233.
[16] Y. Cui, B. Ren, J.-L. Yao, R.-A. Gu, Z.-Q. Tian, Synthesis of AgcoreAushell bimetallic nanoparticles for immunoassay based on surface-enhanced Raman spectroscopy, J. Phys. Chem. B 110 (2006) 4002–4006.
[17] Y. Xie, Y. Jin, Y. Zhou, Y. Wang, SERS activity of self-cleaning silver/titania nanoarray, Appl. Surf. Sci. 313 (2014) 549–557.
[18] C. Xu, X. Wang, Fabrication of flexible metal-nanoparticle films using graphene oxide sheets as substrates, Small 5 (2009) 2212–2217.
[19] G. Amarandei, C. O'Dwyer, A. Arshak, D. Corcoran, Fractal patterning of nanoparticles on polymer films and their sers capabilities, ACS Appl. Mater. Interfaces 5 (2013) 8655–8662.
[20] M. Park, C.S. Hwang, K.-H. Jeong, Nanoplasmonic alloy of Au/Ag nanocomposites on paper substrate for biosensing applications, ACS Appl. Mater. Interfaces 10 (2017) 290–295.
[21] J. Liu, J. Zhou, B. Tang, T. Zeng, Y. Li, J. Li, Y. Ye, X. Wang, Surface enhanced Raman scattering (SERS) fabrics for trace analysis, Appl. Surf. Sci. 386 (2016) 296–302.
[22] S.A. Ogundare, W.E. van Zyl, A Review of Cellulose-Based Substrates for SERS: Fundamentals, Design Principles, Applications, Cellulose, 2019, pp. 1–40.
[23] Z. Xiong, M. Lin, H. Lin, M. Huang, Facile synthesis of cellulose nanofiber nanocomposite as a SERS substrate for detection of thiram in juice, Carbohydr. Polym. 189 (2018) 79–86.
[24] Z. Xiong, X. Chen, P. Liou, M. Lin, Development of nanofibrillated cellulose coated with gold nanoparticles for measurement of melamine by SERS, Cellulose 24 (2017) 2801–2811.
[25] Y. Ma, M. Hummel, M. Määttänen, A. Särkilahti, A. Harlin, H. Sixta, Upcycling of waste paper and cardboard to textiles, Green Chem. 18 (2016) 858–866.
[26] Z.-h. Liu, Y. Kanjo, S. Mizutani, Removal mechanisms for endocrine disrupting compounds (EDCs) in wastewater treatment—physical means, biodegradation, and chemical advanced oxidation: a review, Sci. Total Environ. 407 (2009) 731–748.
[27] H. Fromme, T. Küchler, T. Otto, K. Pilz, J. Müller, A. Wenzel, Occurrence of phthalates and bisphenol A and F in the environment, Water Res. 36 (2002) 1429–1438.
[28] Y. Wang, G. Na, H. Zong, X. Ma, X. Yang, J. Mu, L. Wang, Z. Lin, Z. Zhang, J. Wang, Applying adverse outcome pathways and species

sensitivity−weighted distribution to predicted-no-effect concentration derivation and quantitative ecological risk assessment for bisphenol A and 4-nonylphenol in aquatic environments: a case study on Tianjin City, China, Environ. Toxicol. Chem. 37 (2018) 551−562.

[29] K.A. Fenlon, A.C. Johnson, C.R. Tyler, E.M. Hill, Gas−liquid chromatography−tandem mass spectrometry methodology for the quantitation of estrogenic contaminants in bile of fish exposed to wastewater treatment works effluents and from wild populations, J. Chromatogr. A 1217 (2010) 112−118.

[30] R.B.P. Vidal, G.A. Ibañez, G.M. Escandar, Chemometrics-assisted cyclodextrin-enhanced excitation−emission fluorescence spectroscopy for the simultaneous green determination of bisphenol A and nonylphenol in plastics, Talanta 143 (2015) 162−168.

[31] J.L. Coughlin, B. Winnik, B. Buckley, Measurement of bisphenol A, bisphenol A ß-d-glucuronide, genistein, and genistein 4′-ß-d-glucuronide via SPE and HPLC-MS/MS, Anal. Bioanal. Chem. 401 (2011) 995−1002.

[32] N. Zehani, P. Fortgang, M.S. Lachgar, A. Baraket, M. Arab, S.V. Dzyadevych, R. Kherrat, N. Jaffrezic-Renault, Highly sensitive electrochemical biosensor for bisphenol A detection based on a diazonium-functionalized boron-doped diamond electrode modified with a multi-walled carbon nanotube-tyrosinase hybrid film, Biosens. Bioelectron. 74 (2015) 830−835.

[33] J. Feng, L. Xu, G. Cui, X. Wu, W. Ma, H. Kuang, C. Xu, Building SERS-active heteroassemblies for ultrasensitive Bisphenol A detection, Biosens. Bioelectron. 81 (2016) 138−142.

[34] L. Yang, Y. Chen, Y. Shen, M. Yang, X. Li, X. Han, X. Jiang, B. Zhao, SERS strategy based on the modified Au nanoparticles for highly sensitive detection of bisphenol A residues in milk, Talanta 179 (2018) 37−42.

[35] Y. Ma, S. Asaadi, L.S. Johansson, P. Ahvenainen, M. Reza, M. Alekhina, L. Rautkari, A. Michud, L. Hauru, M. Hummel, High-strength composite fibers from cellulose−lignin blends regenerated from ionic liquid solution, ChemSusChem 8 (2015) 4030−4039.

[36] L.K. Hauru, Y. Ma, M. Hummel, M. Alekhina, A.W. King, I. Kilpeläinen, P.A. Penttilä, R. Serimaa, H. Sixta, Enhancement of ionic liquid-aided fractionation of birchwood. Part 1: autohydrolysis pretreatment, RSC Adv. 3 (2013) 16365−16373.

[37] P. Lee, D. Meisel, Adsorption and surface-enhanced Raman of dyes on silver and gold sols, J. Phys. Chem. 86 (1982) 3391−3395.

[38] L. Castellanos, C. Blanco-Tirado, J. Hinestroza, M. Combariza, In situ synthesis of gold nanoparticles using fique natural fibers as template, Cellulose 19 (2012) 1933−1943.

[39] A. Henglein, M. Giersig, Formation of colloidal silver nanoparticles: capping action of citrate, J. Phys. Chem. B 103 (1999) 9533−9539.

[40] S.A. Ogundare, W.E. van Zyl, Amplification of SERS “hot spots” by silica clustering in a silver-nanoparticle/nanocrystalline-cellulose sensor applied in malachite green detection, Colloid. Surf. Physicochem. Eng. Asp. 570 (2019) 156−164.

[41] Y.-F. Huang, H.-P. Zhu, G.-K. Liu, D.-Y. Wu, B. Ren, Z.-Q. Tian, When the signal is not from the original molecule to be detected: chemical transformation of para-aminothiophenol on Ag during the SERS measurement, J. Am. Chem. Soc. 132 (2010) 9244−9246.

[42] M. Dendisová, L.s. Havránek, M. Oncák, P. Matejka, In situ SERS study of azobenzene derivative formation from 4-aminobenzenethiol on gold, silver, and copper nanostructured surfaces: what is the role of applied potential and used metal? J. Phys. Chem. C 117 (2013) 21245−21253.

[43] L. Kang, P. Xu, B. Zhang, H. Tsai, X. Han, H.-L. Wang, Laser wavelength-and power-dependent plasmon-driven chemical reactions monitored using single particle surface enhanced Raman spectroscopy, Chem. Commun. 49 (2013) 3389−3391.

[44] https://eur-lex.europa.eu/legal-content/EN/TXT/?qid=1518595581058&uri=CELEX:32018R0213, 2018.

[45] W. Xie, S. He, L. Xia, H. Zhang, W. Zhang, Z. Shen, X. Liu, J. Hu, Fabrication of a trans-scale bimetallic synergistic enhanced Raman scattering substrate with high surface-enhanced Raman scattering activity, Anal. Methods 7 (2015) 1676−1679.